Oxygen isotope effect in math xmlns="http://www.w3.org/1998/Math/MathML">mrow>msub>mi mathvariant="normal">VO/mi>mn>2/mn>/msub>/mrow>/math>

Carl Willem Rischau, Xu He, Giacomo Mazza, Stefano Gariglio, Jean-Marc Triscone, Philippe Ghosez, and Javier del Valle

Phys. Rev. B **107**, 115139 — Published 20 March 2023

DOI: 10.1103/PhysRevB.107.115139

Oxygen isotope effect in VO_2

Carl Willem Rischau[1], Xu He[2], Giacomo Mazza[1,3], Stefano Gariglio[1], Jean-Marc Triscone[1], Philippe Ghosez[4] and Javier del Valle[*1,5]

[1]Department of Quantum Matter Physics, University of Geneva, 24 Quai Ernest-Ansermet, 1211 Geneva, Switzerland
[2]Institute of Condensed Matter and Nanosciences, Université Catholique de Louvain, 1348 Louvain-la-Neuve, Belgium
[3] Dipartimento di Fisica, Università di Pisa, Largo Bruno Pontecorvo 3, 56127, Pisa, Italia
[4]Theoretical Materials Physics, CESAM, University of Liège, Liège, Belgium.
[5]Department of Physics, University of Oviedo, C/ Federico García Lorca 18, 33007 Oviedo, Spain

*Corresponding author: javier.delvalle@uniovi.es

Abstract

We investigate the oxygen isotope effect on the VO_2 metal-insulator transition. Using a novel method, we synthetize $V^{16}O_2$ and $V^{18}O_2$ crystals, finding a 1-3% phonon softening and a 1.3 K increase in the metal-insulator transition temperature for the latter. A simple calculation, further confirmed by density functional theory, shows that this shift can be attributed to changes in the lattice internal energy. Our results show that lattice dynamics play a key role at setting the electronic transition temperature, indicating that electronic and structural degrees of freedom remain strongly coupled at the transition.

Introduction

The metal-insulator transition (MIT) is one of the most actively studied topics in condensed matter physics, both for its intrinsic fundamental interest [1–4] as well as for potential applications [5–8]. Among the many materials featuring this phenomenon, VO_2 is arguably the one which has attracted the greatest attention [9]. As temperature is increased above 68 ºC, VO_2 features concomitant electronic and structural transitions, evolving from a monoclinic insulator into a rutile metal [1,9]. In the monoclinic phase, vanadium atoms are dimerized into pairs. Goodenough initially suggested that this dimerization was responsible for the opening of a gap and the emergence of an insulating state [10]. It was later shown that dimerization alone cannot fully explain the gap, without also considering electron-electron correlations [11]. The idea that VO_2 is a 'Peierls-assisted Mott insulator' (or vice versa) became widely accepted [12–16]. In this picture, both structural distortions and electron-electron repulsion are needed to explain the insulating state.

However, in recent years many works have claimed a decoupling between electronic and lattice degrees of freedom, not only in VO_2 but in V_2O_3 as well. Such decoupling is often measured as a transient effect following ultrafast photoexcitation [17–19]. But in many cases, it can also be observed in equilibrium [20–26] or quasi-equilibrium conditions [27]: within a narrow temperature range around the MIT, a monoclinic metallic state is claimed. Upon heating, the

system first undergoes a transition into the metallic state and, a few K later, a structural transition into the rutile lattice [20]. In contrast to this, other works have reported that, when metallic/insulating phase fractions are carefully accounted for, no decoupling is observed [28,29], even in ultrafast timescales [30].

An important piece of the transition puzzle is the influence of lattice dynamics i.e. the role phonons play at setting the transition temperature. Since the VO_2 MIT takes place at relatively high temperatures, phonons can carry an important portion of the system´s total entropy and internal energy. Indeed, Budai *et al*. [2] showed that they contribute 2/3 of the total entropy change across the MIT, with some works increasing that value to over 80% [31]. Isotope effect has traditionally been a common tool to experimentally assess the influence of phonons on electronic phase transitions [32–35]. In the 1970s, Terukov *et al*. [36] reported a small (<1 K), positive oxygen isotope effect in partially substituted (21%) VO_2. However, the samples were not stoichiometrically pure, the effect on the vibrational properties of the material was not reported and its effect on the free energy of the system could not be established.

Here, we use a novel method to synthetize pure, single crystals of $V^{16}O_2$ and fully substituted $V^{18}O_2$. We find that the MIT is 1.3 K higher for $V^{18}O_2$. Raman measurements show a general lattice softening in the 1-3% range for $V^{18}O_2$ compared to $V^{16}O_2$. The sign and magnitude of the observed MIT shift can be accounted for by considering only changes to the lattice free energy, after performing a simple calculation. Our estimation is even more accurate if we take advantage of DFT simulations. These results show that phonons play a key role at setting the electronic transition temperature, supporting the view of a MIT with strongly coupled electronic and lattice degrees of freedom.

Synthesis of $V^{16}O_2$ and $V^{18}O_2$ single crystals

The most common way to fabricate a sample with ^{18}O is by first synthetizing the compound using ^{16}O, and then annealing it at high temperatures in an ^{18}O filled ampoule [37-39]. However, this method would be challenging to realize for VO_2 due to the complex stoichiometric V-O diagram, with many Magnèli phases closely spaced in oxygen content [40]. We take a completely different approach. Recently, Zhao et al. [41] showed that VO_2 single crystal microrods can be fabricated from metallic vanadium foil by applying very large current densities. The process is described in annex A and Figure 4. Joule heating warms the V foil to temperatures up to 1800 ºC. This is enough to oxidize the foil with atmospheric oxygen and to melt the oxidized vanadium. If the current is then suddenly switched off, the liquid VO_X is quenched and VO_2 single crystals nucleate within a V_2O_5 polycrystalline matrix. The V_2O_5 can be removed by submerging it in a Na_2CO_3 solution [41]. This yields clean, single crystal VO_2 rods with lengths up to 300 μm and widths/thicknesses around 10-20 μm, as can be seen in Figure 1a. These rods are hollow with an inner empty space whose size changes from rod to rod. Since all the oxygen is taken from the atmosphere surrounding the vanadium foil, this method offers an excellent opportunity to fabricate $V^{18}O_2$. By following this procedure in a closed environment filled either with $^{16}O_2$ or $^{18}O_2$, we fabricated $V^{16}O_2$ and $V^{18}O_2$ single crystals. X-ray diffraction shows that lattice parameters are the same within experimental resolution (Figures S2 and S3).

Results and discussion

Using silver paste contacts in a four-probe configuration, we characterized the effect of the oxygen isotope on the MIT. This is shown in Figure 1b. The $V^{18}O_2$ sample shows a MIT shifted towards higher temperatures. The sharpness of the transition, common in single crystal VO_2 [3], allows us to accurately determine the MIT temperature and its shift. We must note that Figure 1b plots resistance and not resistivity, since each crystal is different [41] and we have no simple way to calculate the cross section. But that does not hamper the determination of the MIT temperature. Since there is slight sample-to-sample variability, we measured multiple crystals to accumulate statistics. As shown in Figure 1c, we obtain a 1.3±0.3 K higher MIT for $V^{18}O_2$.

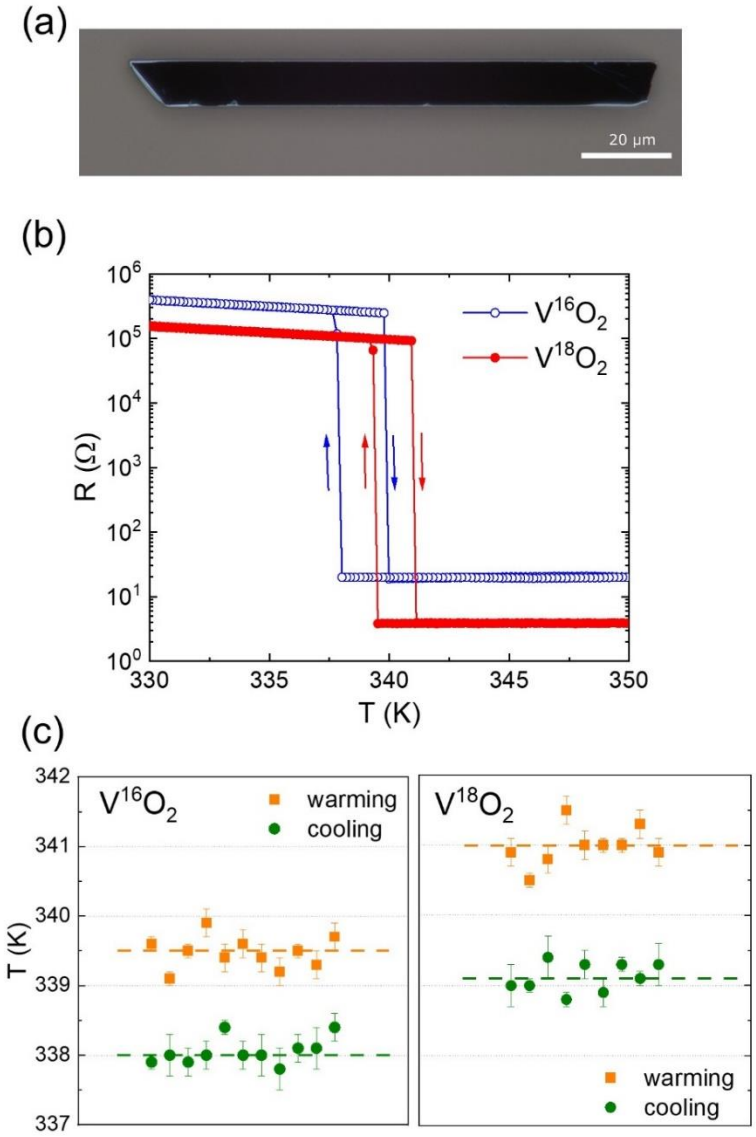

FIG 1. (a) Optical image of a single crystal VO_2 rod. (b) Four-probe resistance vs temperature for $V^{16}O_2$ (empty blue dots) and a $V^{18}O_2$ (red dots) crystals, showing the MIT and the shift due to isotope effect. (c) Transition temperatures for several $V^{16}O_2$ (left panel) and $V^{18}O_2$ (right panel) crystals. Both the warming (orange squares) and cooling (green dots) MIT temperatures are shown. Dotted lines are guides to the eye.

Figures 2a and 2b show Raman spectra of $V^{16}O_2$ and $V^{18}O_2$ crystals in the insulating and metallic state, respectively. The spectra were measured at room temperature with a Horiba LabRAM HR Evolution spectrometer with a wavelength of 532 nm and a spot size between 1 and 2 μm. To measure in the insulating state, a low laser power (0.6 mW) was used to avoid heating. In order to acquire the metallic spectrum, a higher laser power (6 mW) was used, which induced local heating and warmed the sample above the MIT [42]. In both cases a clear phonon softening is observed for $V^{18}O_2$ compared to $V^{16}O_2$. This is to be expected since phonon frequencies generally vary with $1/\sqrt{M}$, being M the isotope mass. The softening is around 3% for phonon modes >30 meV, and less than 1% for lower energy modes. This could be anticipated, since high energy modes in VO_2 are dominated by oxygen motion. Since the softening is proportional to the phonon energy, high energy modes experience a larger effect. For instance, a 3% softening implies that a 50 meV mode is softened by ~1.5 meV, while a 100 meV mode experiences a ~3 meV reduction. The larger softening for higher energy modes is very clear in Figures 2a and 2b.

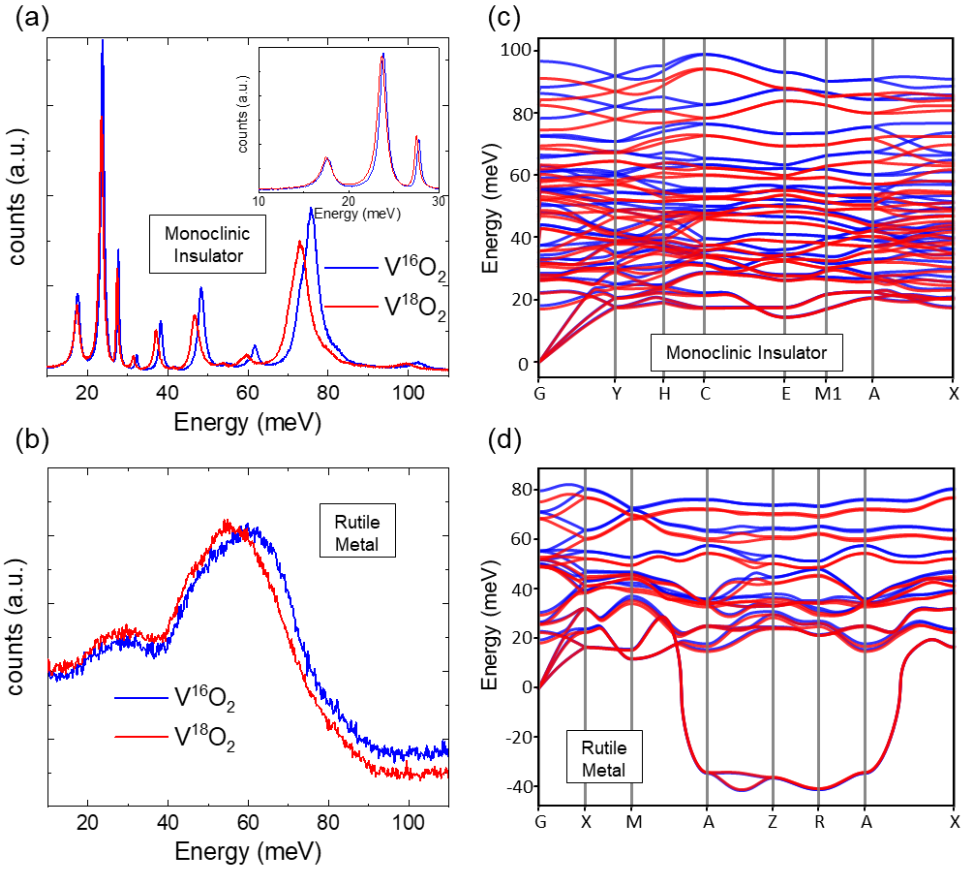

FIG. 2. (a) Raman spectra measured in the insulating phase of $V^{16}O_2$ (blue) and $V^{18}O_2$ (red) crystals. Spectra were captured at room temperature using low laser power to avoid warming up the sample. Inset: Zoom into the low energy phonon region. (b) Raman spectra measured in the metallic phase of $V^{16}O_2$ (blue) and $V^{18}O_2$ (red) crystals. Spectra were captured at room temperature using a high laser power to induce warming above the MIT temperature. (c) DFT-calculated phonon dispersion in the monoclinic insulating phase for $V^{16}O_2$ (blue) and a $V^{18}O_2$ (red). (c) DFT-calculated phonon dispersion of in the rutile metallic phase for $V^{16}O_2$ (blue) and a $V^{18}O_2$ (red). The phonon mode with negative energies is unstable at 0K.

These results are applicable to the whole k-space, as can be seen in the phonon dispersion curves calculated by DFT and shown in Figure 2c and 2d. As in the experiments, phonons are softer for $V^{18}O_2$. The softening is around 3% for phonon energies above 30 meV. As observed in Raman, the softening is larger the higher the mode energy. There is very good agreement between experimental and DFT calculated phonon branches at the Γ point, as shown in Table S1. DFT calculations were done with VASP [43,44] using a PAW approach. A GGA-PBE [45] exchange-correlation functional was used, including a DFT+U correction [46-49]. For the calculation of the phonons we used the Phonopy Package [50]. Further details are discussed in annex 3.

A softening of the overall phonon spectrum implies that the vibrational free energy (F_L) is lower for $V^{18}O_2$ compared to $V^{16}O_2$. But it is lower both for the insulating and the metallic phases, as schematically depicted in Figure 3. To predict the direction of the isotope shift, we need to understand which of the two phases (insulator or metal) experiences a larger reduction in F_L. For this we need to consider the phonon density of states (PDOS). Budai *et al*. [2] measured the VO_2 PDOS using inelastic neutron scattering, finding that it is shifted towards higher energies for the insulating phase i.e. the insulating phase has an overall stiffer lattice. Since the insulator has more high-energy phonon modes, and high-energy modes experience a larger isotope effect (Figure 2), we expect F_L to be lowered more for the insulating state. This makes the insulator thermodynamically more stable and pushes the transition temperature (T_C) up (Fig. 3), as observed in the experiments.

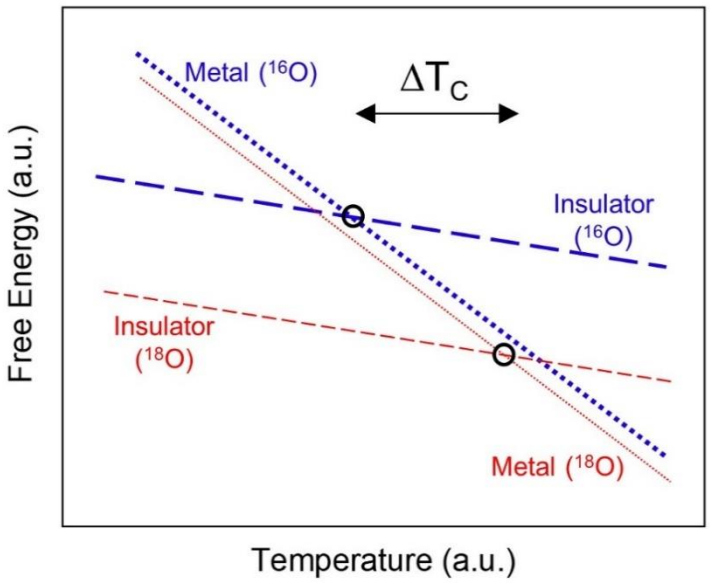

FIG. 3. Schematic representation of free energy vs temperature for the insulating (dashed line) and metallic (dotted line) phases of $V^{16}O_2$ (thick blue lines) and $V^{18}O_2$ (thin red lines). Both the insulating and metallic phases have lower free energies for $V^{18}O_2$, but the reduction is larger for the insulator. This shifts T_C to higher temperatures as depicted. Diagram is not at scale.

Moreover, we can obtain a quantitative estimation of the shift in T_C. At the transition, the free energies of the insulator and the metal are equal, therefore the critical temperature is $T_C = \Delta U/\Delta S$ (*Eq. 1*), where ΔU and ΔS are the total change of internal energy and entropy across the MIT, respectively. Starting from this expression, it is easy to obtain a relationship between the critical temperatures for $V^{16}O_2$ (T_C^{16}) and $V^{18}O_2$ (T_C^{18}):

$$T_C^{18} = \frac{\Delta U^{18}}{\Delta S^{18}} = \frac{\Delta U^{16} + \delta U}{\Delta S^{16} + \delta S} = T_C^{16}\left(\frac{1 + \delta U/\Delta U^{16}}{1 + \delta S/\Delta S^{16}}\right) \qquad (Eq. 2)$$

Where $\delta U = \Delta U^{18} - \Delta U^{16}$ and $\delta S = \Delta S^{18} - \Delta S^{16}$ represent, respectively, the variation in internal energy and entropy changes due to the different isotopes. In principle, both electronic and ionic degrees of freedom contribute to ΔU and ΔS. However, since lattice parameters and bond angles are the same for $V^{16}O_2$ and $V^{18}O_2$ (Figures S2 and S3), we assume that δU and δS are determined solely by changes in lattice dynamics. Therefore:

$$\delta U = \int d(\hbar\omega)\ u \cdot [(D_R^{18} - D_M^{18}) - (D_R^{16} - D_M^{16})] \quad (Eq. 3a)$$

$$\delta S = \int d(\hbar\omega)\ s \cdot [(D_R^{18} - D_M^{18}) - (D_R^{16} - D_M^{16})] \quad (Eq. 3b)$$

Where u and s are the phonon modes energies and entropies, calculated using the well-known formulas:

$$n = \frac{1}{(e^{\hbar\omega/kT} - 1)}\ ;\ u = \left(n + \frac{1}{2}\right)\hbar\omega;\quad s = k\,[(n+1)\ln(n+1) - n\ln n] \quad (Eqs. 4\ a, b\ and\ c)$$

Where n is the mode occupancy and $\hbar\omega$ is the single phonon energy of the mode. Meanwhile D_R^{18}, D_M^{18}, D_R^{16} and D_M^{16} in eq. 3 are the PDOS of the metallic rutile (R) and insulating monoclinic (M) phases, for $V^{18}O_2$ and $V^{16}O_2$, respectively. D_R^{16} and D_M^{16} are extracted directly from the experimental data by Budai *et al*. [2]. D_R^{18} and D_M^{18} are estimated by considering a lattice softening of 3% for $\hbar\omega$ > 30 meV and 0.8% for $\hbar\omega$ < 30 meV.

With that approximation, we obtain $\delta U = 0.13 \pm 0.05$ meV/atom and $T_C\delta S = 0.025 \pm 0.003$ meV/atom. The change in lattice free energy is therefore driven mostly by changes in its internal energy, rather than its entropy. Inserting these results into equation 2, and using the experimental values of ΔU and ΔS [2], we get $T_C^{18} - T_C^{16} = +2.5 \pm 1.2\ K$, which is remarkably similar to our experiments.

The above calculation uses a crude approximation to estimate the $V^{18}O_2$ PDOS from the experimental data: we considered that for $V^{18}O_2$, all phonon branches are 3% softer above 30 meV, and 0.8% below 30 meV. But actually, not all branches are equally softer: the Raman mode at 102 meV is 2.9% softer for $V^{18}O_2$, while the one at 76 meV is 3.6% softer (see Table S1). Following a similar reasoning as in the above estimation, we used the DFT-simulated PDOS for $V^{16}O_2$ and $V^{18}O_2$ to obtain $\delta U = 0.10$ meV/atom and $T_C\delta S = 0.031$ meV/atom. These values yield $T_C^{18} - T_C^{16} = +1.5\ K$. This calculation, further detailed in annex D, is of the order of the experimental

value, and supports our initial estimation. We must note that the unstable branch in the rutile phase is not included in this calculation. This branch, however, experiences a negligible softening.

We must acknowledge that DFT calculations were done without considering anharmonicity or other factors such as electron polarization, which could have yielded a more accurate PDOS. However, to obtain an estimate of the isotope effect it suffices to obtain an approximate description of both phases, and properly determine the effect of changing oxygen isotope. We must note that all phonon calculations were performed at T=0. It is possible to calculate the phonon dispersion at finite temperatures [51], but as has been recently shown [52] that the effect of temperature has only a mild effect on the high frequency phonon modes, which are the ones most affected by the change in oxygen isotope.

For the above calculations we considered the electronic degrees of freedom unaffected by the change in oxygen isotope. This was initially justified by XRD (Figs. 5 and 6), which shows similar static structures for $V^{18}O_2$ and $V^{16}O_2$. However, electron-phonon coupling -which depends linearly on phonon frequency- is expected to introduce a correction to the total system energy. Contrary to what is observed in phase transitions triggered by electron-phonon coupling, such as charge density waves [53], VO_2 shows a very weak mode softening as the transition temperature is approached [2]. The energy of the V-V mode associated with dimerization decreases around 2 meV over an 800 K range. Using this 2 meV value as a crude estimate for the energy due electron-phonon coupling, we would expect a correction to δU in the order of -0.02 meV/atom, well below the contribution of pure lattice degrees of freedom. We note that electron-phonon coupling would reduce the energy of the rutile metal while increasing its entropy, and would therefore push T_C towards negative values, contrary to what we observe.

Experimentally, ΔU is found to be 14.4 meV/atom [2]. Considering only lattice effects, we estimated δU from isotope effect to be 0.13 meV/atom. This is around 1% of ΔU. Since $T_C = \Delta U/\Delta S$, such change would shift T_C around 1%. This is indeed comparable with our experimental results, implying that vibrational energies and entropies play a major role at determining the MIT temperature, at least comparable to that coming from electronic degrees of freedom. This is in accordance with estimations from Budai *et al.* [2] and does not support a scenario with decoupled electronic and structural transitions. If the two transitions took place independently, their associated ΔU and ΔS would be very different [2][31], and their $T_C = \Delta U/\Delta S$ would therefore lay in rather different ranges. This is not what it is observed in experimental reports of decoupled transitions, which take place within a temperature range smaller than 10 K (<3% of 340 K) [20–22]. Moreover, an independent MIT would not be expected to feature an isotopic T_C shift of the magnitude and direction reported here.

Conclusions

Using a novel method [41], we synthetized $V^{16}O_2$ and $V^{18}O_2$ single crystals to study oxygen isotope effect, finding that the MIT takes place 1.3 K higher for $V^{18}O_2$. We used Raman measurements and DFT calculations to determine the isotope influence in lattice dynamics, finding a 1-3% lattice softening for $V^{18}O_2$ samples.

To understand these results, we analyzed the effect that changing oxygen isotope would have on T_C, considering only contributions from changes in lattice internal energy and entropy. A lattice softening reduces the free energy of all phonon modes, this reduction being larger for higher energy

modes. Since in VO_2 the insulating phase has more high energy phonon modes than the metallic phase [2], the total lattice free energy is reduced more for the insulator than for the metal. This results in a higher MIT temperature for $V^{18}O_2$, as experimentally observed. Furthermore, we quantitatively estimated the shift in T_C due to isotope effect both with a simple calculation as well as with DFT, reaching an excellent agreement with our experiments.

Our results underline the importance of lattice dynamics at determining the MIT temperature. They support a scenario in which lattice and electronic degrees of freedom remain tightly coupled across the MIT. Our analysis is simple and general, and could be applicable to other materials, helping explain other reports of isotope effects and clarifying the role that lattice vibrations play on different phase transitions.

Acknowledgements

We thank Marco Lopes for his support during the fabrication and measurement of these samples. We also thank Lukas Korosec and Adriano Amaricci for insightful discussions. This work was funded by the Swiss National Science Foundation through an Ambizione Fellowship (#PZ00P2_185848). C.W.R. was supported by the U.S. Office of Naval Research through the NICOP Grant N62909-21-1-2028. XH and PG acknowledge financial support from F.R.S.-FNRS through the PDR project PROMOSPAN (Grant No. T.0107.20). GM was supported by the Swiss National Science Foundation through an Ambizione Fellowship (Grant No. PZ00P2_186145) and by the MUR-Italian Ministry of Research under the Rita-Levi Montalcini program. Computational resources have been provided by the supercomputing facilities of the Université catholique de Louvain (CISM/UCL) and the Consortium des Équipements de Calcul Intensif en Fédération Wallonie Bruxelles (CÉCI) funded by the F.R.S.-FNRS Belgium (Grant No. 2.5020.11) and the Tier-1 supercomputer of the Fédération Wallonie-Bruxelles funded by the Walloon Region (Grant No. 1117545). J.d.V acknowledges support from the Spanish Ministry of Science through a Ramón y Cajal Fellowship (#RYC2021-030952-I) and from Asturias FICYT under grant AYUD/2021/51185 with the support of FEDER funds.

Appendix A: Synthesis of $V^{16}O_2$ and $V^{18}O_2$ single crystals.

Samples have been grown by thermal oxidation via resistive heating of a piece of Vanadium foil as reported by Zhao et al. [41]. The V foil (99.9 wt% pure, thickness 0.2 mm) was cut into pieces of around 20-30 x 6 mm^2 and connected to a high current source (Lakeshore Model 625) using two clamps in the home-built setup shown in Fig. 4a. The current was gradually increased up to a maximum current of 30 – 40 A (depending on the size of the V foil) until the V became incandescent, and was then abruptly switched off. Fig. 4b shows the color changes of the V foil upon increasing the current through the foil. As the current is increased the V surface oxidizes and turns black. Further increase of the current i.e. temperature melts the oxidized V and liquid drops of VO_x form on both sides of the foil. As the current is switched off abruptly, the liquid VO_x cools down rapidly and crystallizes into VO_2 microtubes on top of a V_2O_5 matrix (see [41] for more details). For the fabrication of $V^{18}O_2$ microtubes the setup was inserted inside the vacuum chamber shown in Fig. 4c that was pumped and then filled with 0.3 bar of $^{18}O_2$ gas. A transparent window in the chamber allowed to observe the color changes of the V foil upon heating. Fig. 4d shows a

top-view optical microscopy image of the solidified droplet with VO_2 microrods grown on top of it. SEM images of the microrods are depicted in Fig. 4e and f, and show an array of hollow rods. Residual V_2O_5 solidified on the walls of the tubes was removed by submerging the as-fabricated product for 30 min in an 30g/l aqueous solution of sodium carbonate Na_2CO_3 ($V_2O_5 + Na_2CO_3 \rightarrow 2NaVO_3 + CO_2$).

Electrical transport measurements were done in a 4-point geometry using a Quantum Design PPMS with electrical contacts done by silver paste.

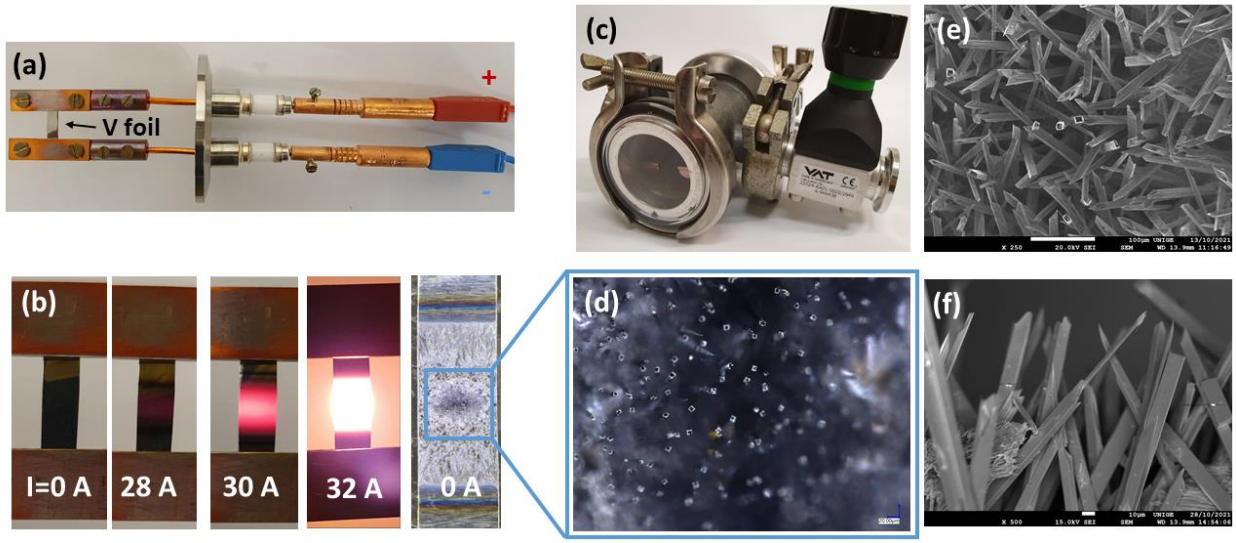

FIG. 4. (a) Home-built setup to heat the V foil by resistive heating. (b) Color changes of the V foil upon increasing the electric current through the V foil. (c) Vacuum chamber that can host the setup shown in panel a, and be filled with $^{18}O_2$ gas. (d) Optical microscopy image showing the VO_2 microtubes grown on top of the V foil. (e) Top and (f) side-view SEM image of grown microtube arrays.

Appendix B: X-ray diffraction of $V^{16}O_2$ and $V^{18}O_2$.

We performed X-ray diffraction to verify that the crystal structure of the $V^{16}O_2$ and the $V^{18}O_2$ samples is identical. In order to get enough counts during the measurements, we detached the VO_X matrix (shown in Fig. 4d) from multiple vanadium foils, and crushed them together. The resulting product is a mixture of polycrystalline V_2O_5 and VO_2 single crystals.

Figure 5 shows the X-ray diffraction patterns of samples synthetized in $^{16}O_2$ (top) and $^{18}O_2$ (bottom) atmospheres. A mixture of VO_2 and V_2O_5 peaks is observed, as expected. Panels in Figure 6 show zoom in views of different 2Θ ranges of the measurement. The position of the peaks is the same within experimental resolution, indicating that our $V^{16}O_2$ an $V^{18}O_2$ samples have identical crystal structure. That is also the case for the $V_2{}^{16}O_5$ and $V_2{}^{18}O_5$ polycrystalline matrix.

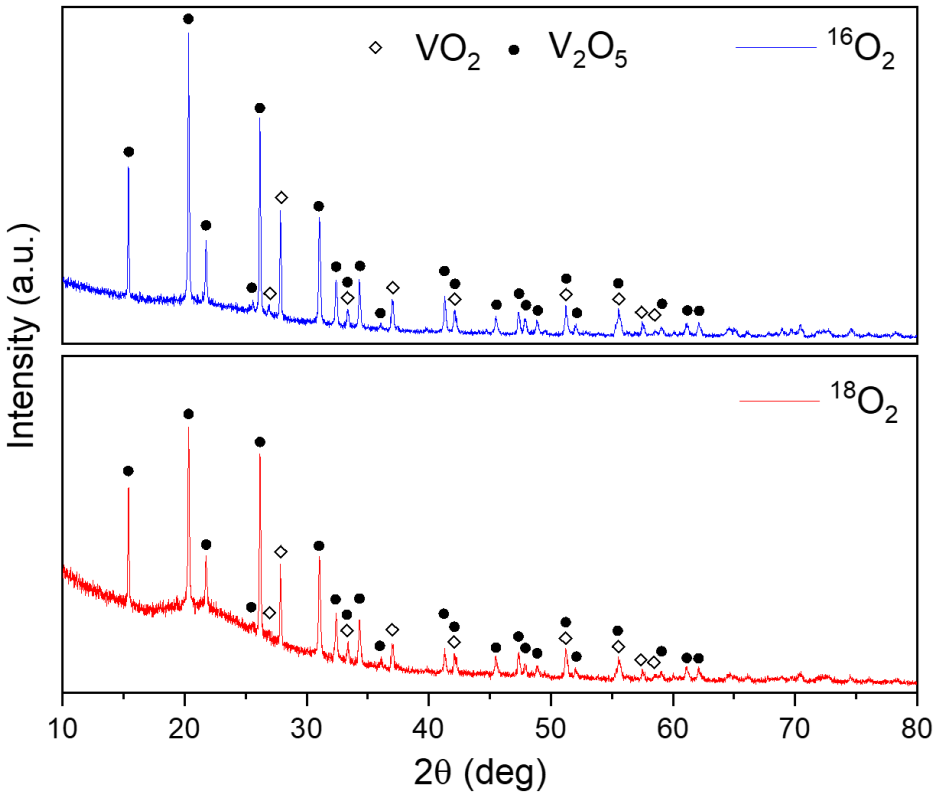

FIG. 5. X-ray diffraction of VO_X samples synthetized in $^{16}O_2$ (top) and $^{18}O_2$ (bottom) atmospheres.

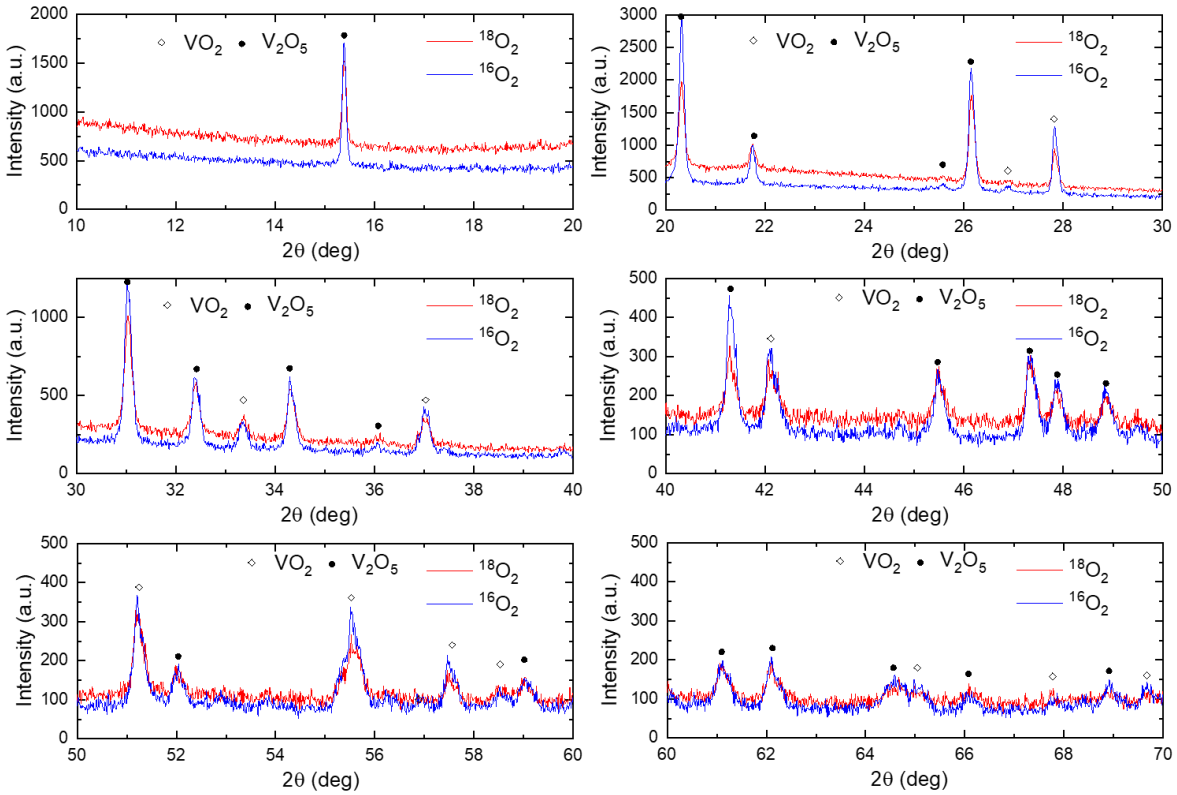

FIG. 6. Zoom in into different 2Θ ranges of the X-ray diffraction measurement of the $V^{16}O_X$ (blue) and $V^{18}O_X$ (red) samples.

Appendix C: DFT simulations.

DFT calculations were done with VASP [53] using a PAW approach, taking an energy cutoff of 500 eV for the plane wave basis set and a 12 × 12 × 12 Monkhorst-Pack k-point mesh sampling for Brillouin zone integrations. We used the GGA-PBE [45] exchange-correlation functional and include a DFT+U correction, with $U\ (V) = 5.2eV$ and $J\ (V) = 0.8eV$. For the calculation of the phonons, entropies and internal energies from the harmonic approximation, we used the frozen phonon method as implemented in the Phonopy Package [50]. The interatomic force constants are computed with a 2 × 2 × 4 supercell. The Raman active irreducible characters of the zone-center phonon modes are identified with the irreps module in Phonopy. The interatomic force constants are not expected to be affected by the isotope effect, so the phonon frequencies with different isotopes are computed by simply varying the atomic mass of oxygen atoms.

There is very good agreement between experimental (Raman) and DFT-calculated phonon branches at the Γ point, as shown in Table 1.

Simulations			**Experiment**		
Frequency (^{16}O) (meV)	**Frequency (^{18}O) (meV)**	**Character**	**Frequency (^{16}O) (meV)**	**Frequency (^{18}O) (meV)**	**Difference ^{16}O -^{18}O (%)**
0	0	A_u			
0	0	B_u			
0	0	B_u			
18.24	17.21	A_g	17.63	17.49	0.8
22.5	22.3	A_u			
26.45	26.22	A_g	23.83	23.64	0.8
26.71	26.65	B_g	27.75	27.49	0.9
27.85	27.23	B_g			
28.58	28.27	A_g			
32.27	30.77	B_u			
32.3	30.95	B_g	32.33	31.52	2.5
33.11	31.62	A_u			
34.52	32.92	A_u			
37.13	35.31	B_u			
37.71	35.87	A_g	38.32	37.17	3
40.05	38.77	B_u			
44.24	43.03	A_u			
46.49	45.44	B_u			
48.11	46.92	A_g	48.4	46.8	3.3
50.38	47.72	A_g			
51.22	48.82	B_g			

55.17	52.16	B_g	55.08	53.73	2.5
55.26	52.47	B_u			
55.88	53.25	A_u			
56.01	54.85	B_g	61.75	59.67	3.4
59.3	56.4	A_u			
61.02	58.17	B_g			
61.7	58.66	A_g			
65.49	61.95	B_u			
65.74	62.15	A_u			
72.68	68.75	B_g			
72.99	69.5	A_g	75.8	73.05	3.6
78.37	74.79	A_g			
86.6	82.73	A_u			
87.07	83.17	B_u			
96.72	91.32	B_g	102.22	99.29	2.9

TABLE 1. Simulated and experimental (Raman) frequencies of the zone-center phonons for ^{16}O and ^{18}O isotopes in the M1 phase. The character of the irreducible presentation of the phonons is identified. The A_g and B_g phonons are Raman active. The frequencies of them are compared with the experimental peaks, showing good agreement.

Appendix D: T_C shift estimation based on the DFT phonon spectra

At the phase transition temperature T_C, there is a free energy crossover between the R and M1 phases. For the ^{16}O and ^{18}O systems (labeled with superscript 0 and 1, respectively), the free energies at T_C are:

$$F^0 = U_R^0 - T_C^0 S_R^0 = U_M^0 - T_C^0 S_M^0, F^0 = U_R^1 - T_C^1 S_R^1 = U_M^1 - T_C^1 S_M^1 \quad \text{(Eq. S1)}$$

where U and S are the internal energy and the entropy, respectively. We take $T_C^0 = 340\ K$.

The internal energy and the entropy come from multiple sources including the lattice vibrations and the thermal fluctuation of the electrons. Most of them are independent of the isotope, and can thus be eliminated when computing the U^1 and S^1 by writing them as the sum of the reference values in the ^{16}O plus an isotope shift.

The internal energy contains the following contributions: (a) the energy at 0 K, which can be represented by the DFT energy, (b) phonon energy due to lattice vibrations U_{ph}, and (c) the energy of electrons due to temperature. Only (b) is directly affected by the isotope effect. Thus, for the M1 phase there is

$$U_M^1 = U_M^0 + \Delta U_{M,ph} \quad \text{(Eq. S2)}$$

where the Δ labels the difference between the ^{18}O and ^{16}O system, the subscript *ph* means phonon.

For the R phase, the $U_{R,ph}$ can be further divided into the contribution from the hard phonons $U_{R,hph}$ and the soft phonons $U_{R,sph}$. The soft phonons are predominantly from V atoms, which are not affected by the isotope effect as shown in Fig. 7. Therefore, we approximate:

$$U_R^1 = U_R^0 + \Delta U_{R,hph} \quad \text{(Eq. S3)}$$

The entropy S contains the phonon and the electron contributions. Only the phonon contribution S_{ph} is directly affected by the isotope effect. Therefore, in the M1 phase,

$$S_M^1 = S_M^0 + \Delta S_{M,ph} \quad \text{(Eq. S4)}$$

In the R phase, the $S_{R,ph}$ can also be decomposed as the contribution from the soft and hard phonons, and only the latter is affected by the isotope effect. Thus,

$$S_R^1 = S_R^0 + \Delta S_{R,hph} \quad \text{(Eq. S5)}$$

From Eqn. S1, there is

$$U_R^0 = U_M^0 + T_C^0(S_R^0 - S_M^0) \quad \text{(Eq. S6)}$$

By plugging equations S2 to S6 into Eq. S1, we arrive at

$$\Delta U_{R,hph} - \Delta U_{M,ph} + T_C^0(S_R^0 - S_M^0) = T_C^1(S_R^0 + \Delta S_{R,hph} - S_M^0 - \Delta S_{M,ph}) \quad \text{(Eq. S7)}$$

which gives:

$$T_C^1 = \frac{1}{1+\alpha}\left[T_C^1 + \frac{\Delta U_{R,hph} - \Delta U_{M,ph}}{S_R^0 - S_M^0}\right] \quad \text{(Eq. S8)}$$

where $\alpha = \frac{\Delta S_{R,hph} - \Delta S_{M,ph}}{S_R^0 - S_M^0}$.

The $U_{R,hph}$, $S_{R,hph}$, $U_{M,ph}$ and $S_{R,ph}$ can be easily obtained as functions of temperature within the harmonic approximation, as shown in Fig. 8.

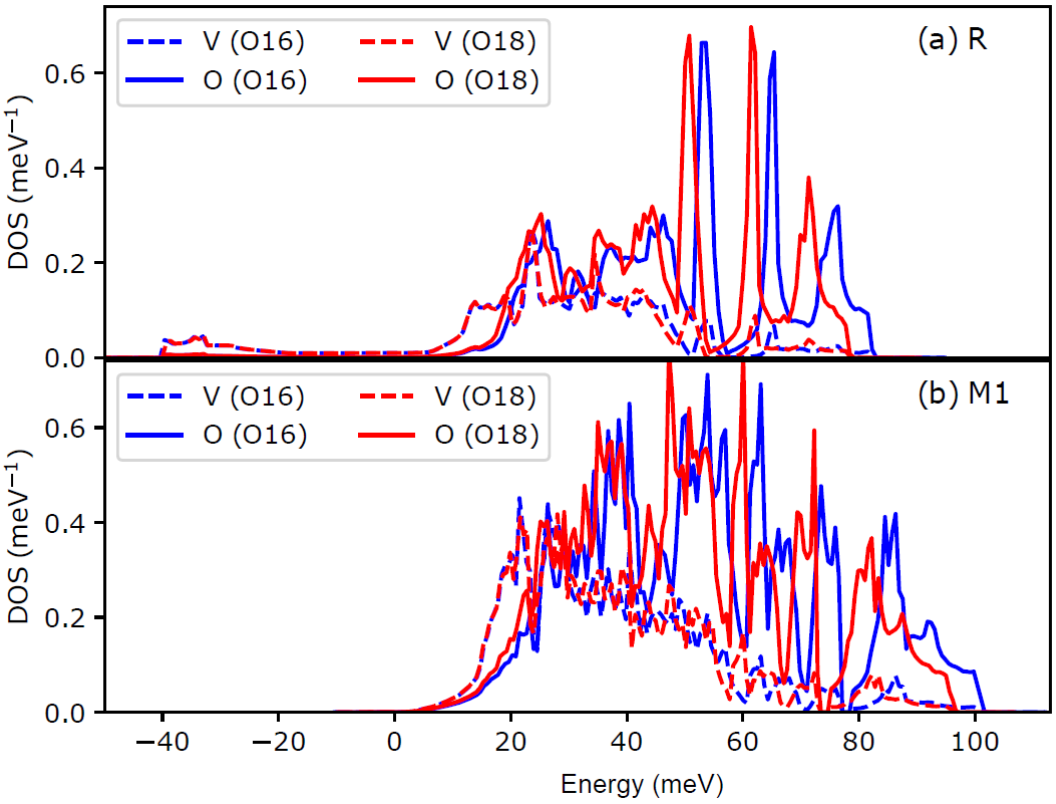

FIG. 7. Phonon density of states projected to the V and O atoms in (a) the rutile phase and (b) the monoclinic phase.

At 340K, The shift of the entropies and internal energies from the harmonic approximation are: $\Delta S_{M,ph}$ = 0.746 J/(K mol) , $\Delta U_{M,ph}$ = -173 J/mol, $\Delta S_{R,hph}$ = 0.774 J/(K mol) , $\Delta U_{R,hph}$ = -144 J/mol. Taking the experimental S_R^0-S_M^0=13 J/(K mol) [2], we get a T_C^1 of 341.5K, i.e. an up shift of ΔT_C = 1.5 K, which agrees very well with the experimental value.

Note that isotope shifts of the phonon entropy in the R and M1 phase almost cancel out ($\Delta S_{R,hph} \approx \Delta S_{M,ph}$). The main contribution to the ΔT_C is mostly from the shifting of the internal energy.

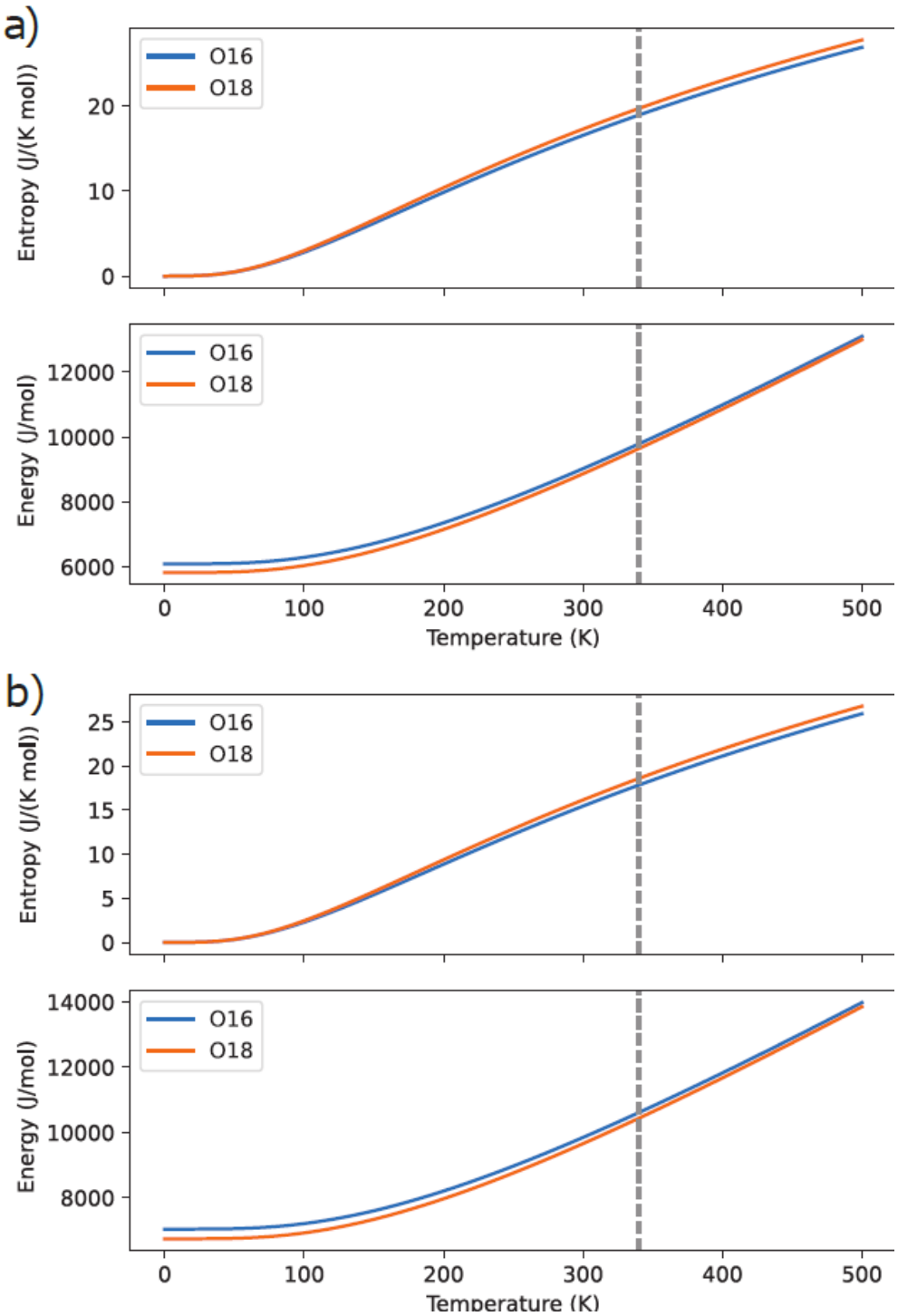

FIG. 8. Entropy and internal energy of VO_2 phonons from the harmonic approximation. (a) In the Rutile phase. Only stable phonons are included in the calculation. (b) In the M1 phase. All phonons are considered in this phase.

References

[1] M. Imada, A. Fujimori, and Y. Tokura, Metal-Insulator Transitions, *Rev. Mod. Phys*. **70**, 1039 (1998).

[2] J. D. Budai, J. Hong, M. E. Manley, E. D. Specht, C. W. Li, J. Z. Tischler, D. L. Abernathy, A. H. Said, B. M. Leu, L. A. Boatner, R. J. Mcqueeney, and O. Delaire, Metallization of vanadium dioxide driven by large phonon entropy, *Nature* **515**, 535-539 (2014).

[3] A. B. Georgescu and A. J. Millis, Quantifying the role of the lattice in metal–insulator phase transitions, *Comm. Phys.* **5**, 135 (2022).

[4] M. A. Davenport, M. J. Krogstad, L. M. Whitt, C. Hu, T. C. Douglas, N. Ni, S. Rosenkranz, R. Osborn, and J. M. Allred, Fragile 3D Order in $V_{1-x}Mo_xO_2$, *Phys. Rev. Lett.* **127**, 125501 (2021).

[5] J. del Valle, N. M. Vargas, R. Rocco, P. Salev, Y. Kalcheim, P. N. Lapa, C. Adda, M.-H. Lee, P. Y. Wang, L. Fratino, M. J. Rozenberg, and I. K. Schuller, Spatiotemporal characterization of the field-induced insulator-to-metal transition, *Science* **373**, 907-911 (2021).

[6] J. del Valle, P. Salev, Y. Kalcheim, and I. K. Schuller, A caloritronics-based Mott neuristor, *Sci. Rep*. **10**, 4292 (2020).

[7] K. Tang, K. Dong, J. Li, M. P. Gordon, F. G. Reichertz, H. Kim, Y. Rho, Q. Wang, C. Y. Lin, C. P. Grigoropoulos, A. Javey, J. J. Urban, J. Yao, R. Levinson, and J. Wu, Temperature-adaptive radiative coating for all-season household thermal regulation, *Science* **374**, 1504 (2021).

[8] S. Cueff, J. John, Z. Zhang, J. Parra, J. Sun, R. Orobtchouk, S. Ramanathan, and P. Sanchis, VO_2 Nanophotonics, *APL Photonics* **5**, 110901 (2020).

[9] F. J. Morin, Oxides Which Show a Metal-to-Insulator Transition at the Neel Temperature, *Phys. Rev. Lett.* **3**, 34 (1959).

[10] J. B. Goodenough, The two components of the crystallographic transition in VO_2, *J. Sol. Stat. Chem*. **3**, 490-500 (1971).

[11] M. W. Haverkort, Z. Hu, A. Tanaka, W. Reichelt, S. V. Streltsov, M. A. Korotin, V. I. Anisimov, H. H. Hsieh, H. J. Lin, C. T. Chen, D. I. Khomskii, and L. H. Tjeng, Orbital-Assisted Metal-Insulator Transition in VO_2, *Phys. Rev. Lett.* **95**, 196404 (2005).

[12] S. Biermann, A. Poteryaev, A. I. Lichtenstein, and A. Georges, Dynamical Singlets and Correlation-Assisted Peierls Transition in VO_2, *Phys. Rev. Lett*. **94**, 026404 (2005).

[13] W. H. Brito, M. C. O. Aguiar, K. Haule, and G. Kotliar, Metal-Insulator Transition in VO_2: A DFT+DMFT Perspective, *Phys. Rev. Lett*. **117**, 056402 (2016).

[14] C. Weber, D. D. O'Regan, N. D. M. Hine, M. C. Payne, G. Kotliar, and P. B. Littlewood, Vanadium Dioxide: A Peierls-Mott Insulator Stable against Disorder, *Phys. Rev. Lett.* **108**, 256402 (2012).

[15] O. Nájera, M. Civelli, V. Dobrosavljević, and M. J. Rozenberg, Resolving the VO_2 controversy: Mott mechanism dominates the insulator-to-metal transition, *Phys. Rev. B* **95**, 035113 (2017).

[16] F. Grandi, A. Amaricci, and M. Fabrizio, Unraveling the Mott-Peierls intrigue in vanadium dioxide, *Phys. Rev. Res.* **2**, 013298 (2020).

[17] V. R. Morrison, R. P. Chatelain, K. L. Tiwari, A. Hendaoui, A. Bruhács, M. Chaker, and B. J. Siwick, A photoinduced metal-like phase of monoclinic VO_2 revealed by ultrafast electron diffraction, *Science* **346**, 445 (2014).

[18] H. T. Kim, Y. W. Lee, B. J. Kim, B. G. Chae, S. J. Yun, K. Y. Kang, K. J. Han, K. J. Yee, and Y. S. Lim, Monoclinic and Correlated Metal Phase in VO_2 as Evidence of the Mott Transition: Coherent Phonon Analysis, *Phys. Rev. Lett*. **97**, 266401 (2006).

[19] S. Wang, J. G. Ramirez, J. Jeffet, S. Bar-Ad, D. Huppert, and I. K. Schuller, Ultrafast photo-induced dynamics across the metal-insulator transition of VO_2, *Europhys. Lett.* **118**, 27005 (2017).

[20] D. Lee, B. Chung, Y. Shi, G. Y. Kim, N. Campbell, F. Xue, K. Song, S. Y. Choi, J. P. Podkaminer, T. H. Kim, P. J. Ryan, J. W. Kim, T. R. Paudel, J. H. Kang, J. W. Spinuzzi, D. A. Tenne, E. Y. Tsymbal, M. S. Rzchowski, L. Q. Chen, J. Lee, and C. B. Eom, Isostructural metal-insulator transition in VO_2, *Science* **362**, 1037 (2018).

[21] J. Laverock, S. Kittiwatanakul, A. Zakharov, Y. Niu, B. Chen, S. A. Wolf, J. W. Lu, and K. E. Smith, Direct Observation of Decoupled Structural and Electronic Transitions and an Ambient Pressure Monocliniclike Metallic Phase of VO_2, *Phys. Rev. Lett*. **113**, 216402 (2014).

[22] M. K. Liu, M. Wagner, E. Abreu, S. Kittiwatanakul, A. McLeod, Z. Fei, M. Goldflam, S. Dai, M. M. Fogler, J. Lu, S. A. Wolf, R. D. Averitt, and D. N. Basov, Anisotropic Electronic State via Spontaneous Phase Separation in Strained Vanadium Dioxide Films, *Phys. Rev. Lett*. **111**, 096602 (2013).

[23] B. J. Kim, Y. W. Lee, S. Choi, J. W. Lim, S. J. Yun, H. T. Kim, T. J. Shin, and H. S. Yun, Micrometer x-ray diffraction study of VO2 films: Separation between metal-insulator transition and structural phase transition, *Phys. Rev. B* **77**, 235401 (2008).

[24] H. Madan, M. Jerry, A. Pogrebnyakov, T. Mayer, and S. Datta, Quantitative Mapping of Phase Coexistence in Mott-Peierls Insulator during Electronic and Thermally Driven Phase Transition, *ACS Nano* **9**, 2009 (2015).

[25] P. Schofield, E. J. Braham, B. Zhang, J. L. Andrews, H. K. Drozdick, D. Zhao, W. Zaheer, R. M. Gurrola, K. Xie, P. J. Shamberger, X. Qian, and S. Banerjee, Decoupling the metal–insulator transition temperature and hysteresis of VO_2 using Ge alloying and oxygen vacancies, *Chem. Commun*. **58**, 6586 (2022).

[26] A. S. McLeod, E. Van Heumen, J. G. Ramirez, S. Wang, T. Saerbeck, S. Guenon, M. Goldflam, L. Anderegg, P. Kelly, A. Mueller, M. K. Liu, I. K. Schuller, and D. N. Basov, Nanotextured phase coexistence in the correlated insulator V_2O_3, *Nat. Phys*. **13**, 80 (2017).

[27] A. Sood, X. Shen, Y. Shi, S. Kumar, S. J. Park, M. Zajac, Y. Sun, L. Q. Chen, S. Ramanathan, X. Wang, W. C. Chueh, and A. M. Lindenberg, Universal phase dynamics in VO_2 switches revealed by ultrafast operando diffraction, *Science* **373**, 352 (2021).

[28] G. J. Paez, C. N. Singh, M. J. Wahila, K. E. Tirpak, N. F. Quackenbush, S. Sallis, H. Paik, Y. Liang, D. G. Schlom, T. L. Lee, C. Schlueter, W. C. Lee, and L. F. J. Piper,

Simultaneous Structural and Electronic Transitions in Epitaxial VO_2/TiO_2 (001), *Phys. Rev. Lett*. **124**, 196402 (2020).

[29] Y. Kalcheim, N. Butakov, N. M. Vargas, M. H. Lee, J. Del Valle, J. Trastoy, P. Salev, J. Schuller, and I. K. Schuller, Robust Coupling between Structural and Electronic Transitions in a Mott Material, *Phys. Rev. Lett*. **122**, 057601 (2019).

[30] L. Vidas, D. Schick, E. Martínez, D. Perez-Salinas, A. Ramos-Álvarez, S. Cichy, S. Batlle-Porro, A. S. Johnson, K. A. Hallman, R. F. Haglund, and S. Wall, Does VO_2 Host a Transient Monoclinic Metallic Phase?, *Phys. Rev. X* **10**, 031047 (2020).

[31] T. A. Mellan, H. Wang, U. Schwingenschlögl and R. Grau-Crespo, Origin of the transition entropy in vanadium dioxide, *Phys. Rev. B* **99**, 064113 (2019).

[32] M. Medarde, P. Lacorre, K. Conder, F. Fauth, and A. Furrer, Giant ^{16}O-^{18}O Isotope Effect on the Metal-Insulator Transition of $RNiO_3$ Perovskites (R = Rare Earth), *Phys. Rev. Lett*. **80**, 2397 (1998).

[33] N. A. Babushkina, L. M. Belova, O. Y. Gorbenko, A. R. Kaul, A. A. Bosak, V. I. Ozhogin, and K. I. Kugel, Metal–insulator transition induced by oxygen isotope exchange in the magnetoresistive perovskite manganites, *Nature* **391**, 159 (1998).

[34] C. A. Reynolds, B. Serin, W. H. Wright, and L. B. Nesbitt, Superconductivity of Isotopes of Mercury, *Phys. Rev.* **78**, 487 (1950).

[35] B. Batlogg, R. J. Cava, A. Jayaraman, R. B. Van Dover, G. A. Kourouklis, S. Sunshine, D. W. Murphy, L. W. Rupp, H. S. Chen, A. White, K. T. Short, A. M. Mujsce, and E. A. Rietman, Isotope Effect in the High-Tc Superconductors $Ba_2YCu_3O_7$ and $Ba_2EuCu_3O_7$, *Phys. Rev. Lett*. **58**, 2333 (1987).

[36] E. I. Terukov, W. Reichelt, M. Wolf, H. Hemschik and H. Oppermann, On the influence of the substitution of O^{16} by O^{18} in a few vanadium oxides on their semiconductor—metal transition, *Phys. Stat. Sol. (a)* **48**, 377 (1978).

[37] C. W. Rischau, D. Pulmannová, G. W. Scheerer, A. Stucky, E. Giannini, and D. van der Marel, Isotope tuning of the superconducting dome of strontium titanate, *Phys. Rev. Res*. **4**, 013019 (2022).

[38] J. Jeong, N. Aetukuri, T. Graf, T. D. Schladt, M. G. Samant, and S. S. P. Parkin, Suppression of Metal-Insulator Transition in VO_2 by Electric Field–Induced Oxygen Vacancy Formation, *Science* **339**, 1402 (2013).

[39] C. Marini, E. Arcangeletti, D. Di Castro, L. Baldassare, A. Perucchi, S. Lupi, L. Malavasi, L. Boeri, E. Pomjakushina, K. Conder, and P. Postorino, Optical properties of $V_{1-x}Cr_xO_2$ compounds under high pressure, *Phys. Rev. B* **77**, 235111 (2008).

[40] U. Schwingenschlögl and V. Eyert, The vanadium Magneli phases $V_nO_{(2n-1)}$, *Ann. Phys*. **13**, 475 (2004).

[41] C. Zhao, S. Ma, Z. Li, W. Li, J. Li, Q. Hou, and Y. Xing, Simple and fast fabrication of single crystal VO_2 microtube arrays, *Commun. Mater*. **1**, 28 (2020).

[42] I. Ardizzone, J. Teyssier, I. Crassee, A. B. Kuzmenko, D. G. Mazzone, D. J. Gawryluk, M. Medarde, and D. Van Der Marel, Raman spectroscopic evidence for multiferroicity in rare earth nickelate single crystals, *Phys. Rev. Res*. **3**, 033007 (2021).

[43] G. Kresse and J. Furthmüller, Efficient iterative schemes for ab initio total-energy calculations using a plane-wave basis set, *Phys. Rev. B* 54, 11169 (1996).

[44] G. Kresse and D. Joubert, From ultrasoft pseudopotentials to the projector augmented-wave method, *Phys. Rev. B* 59, 1758 (1999).

[45] J. P. Perdew, K. Burke, and M. Ernzerhof, Generalized Gradient Approximation Made Simple, *Phys. Rev. Lett*. **77**, 3865 (1996).

[46] A. I. Lichtenstein, V. I. Anisimov and J. Zaanen, Density-functional theory and strong interactions: Orbital ordering in Mott-Hubbard insulators, Phys. Rev. B 52, R5467 (1995).

[47] W. R. Mondal, E. Evlyukhin, S. A. Howard, G. J. Paez, H. Paik, D. G. Schlom, L. F. J. Piper and W.-C. Lee, Role of V-V dimers on structural, electronic, magnetic, and vibrational properties of VO_2 by first-principles simulations and Raman spectroscopic analysis, *Phys. Rev. B* **103**, 214107 (2021).

[48] S. Kim, K. Kim, C.-J. Kang and B. I. Min, Correlation-assisted phonon softening and the orbital-selective Peierls transition in VO_2, *Phys. Rev. B* 87, 195106 (2013).

[49] M. A. Korotin, N. A. Shorikov, and V. I. Anisimov, Calculation of the electronic structure of the vanadium dioxide VO_2 in the monoclinic low-temperature phase M1 using the generalized transition state method, *Phys. Metals Metallograph* (USSR) **94**, 17 (2002).

[50] A. Togo and I. Tanaka, First principles phonon calculations in materials science, *Scr. Mater*. **108**, 1-5 (2015).

[51] X. Zhang, C. Zhang, C. Zhang, P. Zhang, and W. Kang, Finite-temperature phonon dispersion and vibrational dynamics of $BaTiO_3$ from first-principles molecular dynamics, *Phys. Rev. B* **105**, 014304 (2022).

[52] Y. Xia and M. K. Y. Chan, Renormalized Lattice Dynamics and Thermal Transport in VO_2, *arXiv:1711.02819* (2017).

[53] J. Hafner, Ab-initio simulations of materials using VASP: Density-functional theory and beyond, *J. Comput. Chem*. **29**, 2044 (2008).